On the influence of crossing angle on long-term rail damage evolution in railway crossings

Downloaded from: https://research.chalmers.se, 2026-04-06 03:22 UTC

Citation for the original published paper (version of record):

Skrypnyk, R., Pålsson, B., Nielsen, J. et al (2021). On the influence of crossing angle on long-term rail damage evolution in railway crossings. International Journal of Rail Transportation, 9(6): 503-519. http://dx.doi.org/10.1080/23248378.2020.1864794

N.B. When citing this work, cite the original published paper.

research.chalmers.se offers the possibility of retrieving research publications produced at Chalmers University of Technology. It covers all kind of research output: articles, dissertations, conference papers, reports etc. since 2004. research.chalmers.se is administrated and maintained by Chalmers Library

(article starts on next page)

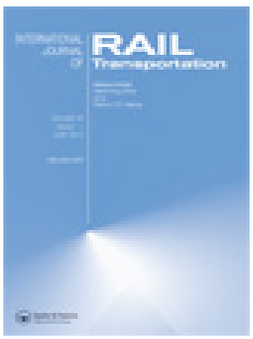

International Journal of Rail Transportation

ISSN: (Print) (Online) Journal homepage: https://www.tandfonline.com/loi/tjrt20

On the influence of crossing angle on long-term rail damage evolution in railway crossings

Rostyslav Skrypnyk , Björn A. Pålsson , Jens C. O. Nielsen & Magnus Ekh

To cite this article: Rostyslav Skrypnyk , Björn A. Pålsson , Jens C. O. Nielsen & Magnus Ekh (2021): On the influence of crossing angle on long-term rail damage evolution in railway crossings, International Journal of Rail Transportation, DOI: 10.1080/23248378.2020.1864794

To link to this article: https://doi.org/10.1080/23248378.2020.1864794

© 2021 The Author(s). Published by Informa UK Limited, trading as Taylor & Francis Group.

Published online: 06 Jan 2021.

Submit your article to this journal

Article views: 131

View related articles

View Crossmark data

Full Terms & Conditions of access and use can be found at
https://www.tandfonline.com/action/journalInformation?journalCode=tjrt20

INTERNATIONAL JOURNAL OF RAIL TRANSPORTATION
https://doi.org/10.1080/23248378.2020.1864794

Taylor & Francis
Taylor & Francis Group

OPEN ACCESS Check for updates

On the influence of crossing angle on long-term rail damage evolution in railway crossings

Rostyslav Skrypnyk[a], Björn A. Pålsson[a], Jens C. O. Nielsen[a] and Magnus Ekh[b]

[a]Department of Mechanics and Maritime Sciences/CHARMEC, Chalmers University of Technology, Gothenburg, Sweden; [b]Department of Industrial and Materials Science/CHARMEC, Chalmers University of Technology, Gothenburg, Sweden

ABSTRACT

The rails in railway crossings are subjected to severe load environment leading to degradation of running surface due to wear and accumulated plastic deformation. To compare long-term degradation of three fixed crossings with different crossing angles, nominally designated 1:12, 1:15, and 1:18.5, a multidisciplinary simulation methodology is applied to predict damage of the crossing rail. For a given traffic scenario, including up to 65 MGT of facing move passenger traffic in through route, the results show that damage increases with increasing crossing angle. The ratio between the maximum damage for the crossings with the largest and smallest crossing angles is found to be about three in terms of wear and about two for plastic deformation. Initially high rate of plastic deformation reduces significantly after the first 2–5 MGT, and after 10–30 MGT it approaches a nearly constant value that is significantly lower than the wear rate.

ARTICLE HISTORY
Received 14 July 2020
Revised 7 December 2020
Accepted 12 December 2020

KEYWORDS
Dynamic vehicle–track interaction; railway crossing; FEM; plastic deformation; wear

1. Introduction

Railway crossings represent a structural and geometrical irregularity in railway track that induces a severe load environment. As a result, frequent maintenance of crossings is required due to damage in the forms of wear, plastic deformation and breaking out of material caused by surface or subsurface initiated rolling contact fatigue cracking. The dynamic wheel–rail interaction in the crossing panel typically results in an impact load on the crossing rail (traffic in facing move) or on the wing rail (trailing move). The magnitudes of these impact loads depend on the dynamics of the system, vehicle speed, axle load and on the impact angle, which is a difference in inclination between the vertical wheel trajectories on the wing rail and crossing rail. Furthermore, worn wheel profiles may contribute significantly to an increase in impact load. If the rail profiles are not corrected in time, they will also contribute to a magnification of the impact loads.

Hence, it is imperative for an infrastructure manager or a turnout manufacturer to have a tool that can aid in the prediction of long-term rail damage and therefore provide guidance regarding turnout design, selection of the material for the crossing and the

CONTACT Rostyslav Skrypnyk rostyslav.skrypnyk@chalmers.se Department of Mechanics and Maritime Sciences/CHARMEC, Chalmers University of Technology, Gothenburg Hörsalsvägen 7A, SE-412 96 Gothenburg, Sweden

© 2021 The Author(s). Published by Informa UK Limited, trading as Taylor & Francis Group.
This is an Open Access article distributed under the terms of the Creative Commons Attribution-NonCommercial-NoDerivatives License (http://creativecommons.org/licenses/by-nc-nd/4.0/), which permits non-commercial re-use, distribution, and reproduction in any medium, provided the original work is properly cited, and is not altered, transformed, or built upon in any way.

frequency of maintenance. Few such tools can be found in the literature. It has been reported in [1] that plastic deformation, wear and rolling contact fatigue (RCF) are the three main damage mechanisms that influence the life of a crossing. This is why it would be preferable if the simulation tool could account for all of these.

A three-dimensional (3D) explicit finite element (FE) model of a single wheelset rolling over a crossing, with a non-linear material model for the rail, has been used in conjunction with a fatigue life model for the prediction of RCF, see, e.g. [2]. and [3]. The advantages with this approach are a more accurate modelling of the wheel–rail contact [4] and the consideration of the non-proportional loading, which leads to additional material hardening [5]. However, due to high computational cost, it has been limited to studies of a single wheel profile rolling over the crossing, which can have a significant influence on the contact conditions [6] and the calculated distribution of damage. Additionally, very few studies adopting this approach have considered all three main damage mechanisms [7]. An alternative approach is to combine a multibody dynamics model with a simplified contact model to simulate the dynamic train–track interaction and then compute one (wear, see [8]) or several (wear, plastic deformation and RCF, see [9]) damage mechanisms in a postprocessing step. The advantage of this approach is that it alleviates the computational cost and allows for the variation in traffic conditions, such as wheel profiles, vehicle speeds and wheel–rail friction coefficients, to be accounted for.

The geometrical design of a crossing has a critical influence on the vehicle dynamics. For example, it was shown in [10] that a movable crossing rail design can reduce the impact loads in the crossing zone. Another study [11] considered a new design approach where a single piece crossing rail was elastically mounted on the rest of the casting. The aim of the present study is to compute the influence of the crossing angle on the long-term performance of fixed crossings in terms of plastic deformation and wear. For a given traffic scenario, it is known from field experience that a larger crossing angle α (see Figure 1) results in more damage compared to a smaller one. In this paper, this aggravation of damage will be quantified by applying the simulation methodology to three crossings with different crossing angles.

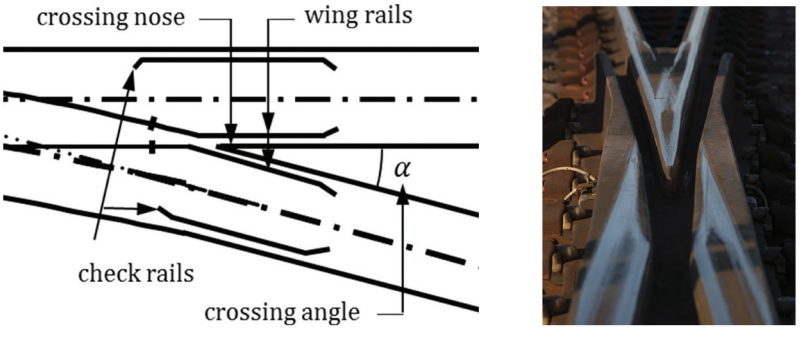

Figure 1. Components of crossing panel (left) and photo of a fixed crossing (right). Adopted from [12].

2. Simulation methodology

The present study uses the multidisciplinary iterative methodology presented in [9]. Since the time of its original publication, the methodology has been improved in terms of computational efficiency and robustness (see [6,13]). The methodology predicts the rail damage at sampled cross-sections along the crossing rail. It is comprised of the following steps:

(1) Simulation of dynamic vehicle–track interaction by means of a commercial multi-body simulation (MBS) software to predict wheel–rail contact forces, creepages, and contact positions. The simulations may account for stochastic variations of several input parameters, such as vehicle speed and wheel–rail friction. This was demonstrated using Latin hypercube sampling in [9] and [14]. In this study, the stochastic input data are limited to the variation in worn wheel profiles to ensure a spread of contact locations on the crossing rail, while keeping focus on the influence of the crossing angle. N_1 vehicles (each having N_{axle} axles and a unique wheel profile; see Figure 2) are considered. The model uses the Hertzian solution for the normal contact and the FASTSIM algorithm [15] for the tangential contact. For wheel–rail contact at the top of a crossing rail, it was shown in [4] that the Hertzian model is sufficiently accurate at low computational cost when compared with two non-elliptical models (Kalker's variational method and the finite element method).

(2) Simulation of normal contact for each wheel–rail contact scenario predicted by the previous step. The output of this step is the contact patch size and the maximum von Mises stress (needed for calculations of plastic deformation in the next step). The normal contact problem is solved only for the sampled cross-sections. Only the rail material is assumed to deform inelastically. It is assumed that the measured worn wheel profiles

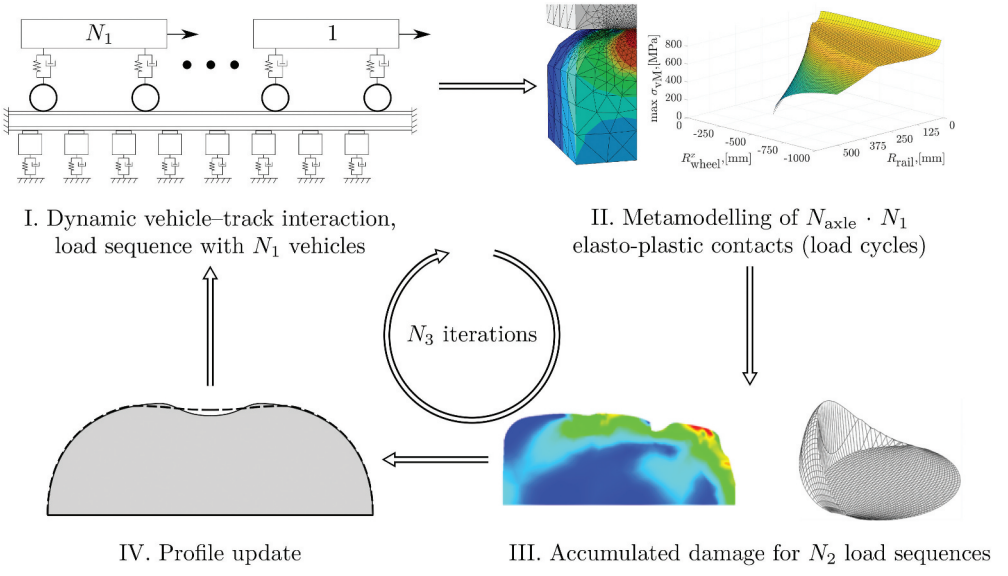

Figure 2. Illustration of iterative simulation methodology (adopted from [6]).

considered in this study have been subjected to initial hardening and have reached elastic shakedown.

The normal contact problem is solved using a Hertzian-based metamodel (see [13]) that has been calibrated against 3D FE simulations of wheel–rail contact with non-linear material properties. The metamodel was calibrated for rail contact radii (in the plane of each rail cross-section) in the interval $[20, 500]$ mm, wheel contact radii in the plane of the wheel cross-section and in the circumferential direction in the intervals $[60, 1000]$ mm and $[450, 480]$ mm, respectively, and normal wheel–rail contact loads in the interval $[100, 300]$ kN, cf. Figure 2. For each load cycle and each rail cross-section, the output from the metamodel is determined by the contact radii at the simulated contact positions on wheel and rail (as in the Hertzian theory of contact), accounting for the updated rail profiles in each iteration step. Thus, the influence of evolving local damage due to wear and plastic deformation is considered. However, the minimum radius of the circle that is used to fit the shape of the rail cross-section at the point of contact is 20 mm. Thus, local rail irregularities with radii smaller than 20 mm are not accounted for properly. Irregularities in the direction along the crossing are not considered in the simulation of normal contact. Replacing the FE simulations with the metamodel leads to a significant reduction of computational time as several hundreds of contact scenarios need to be solved within each iteration corresponding to 0.05 MGT of simulated traffic, making it possible to simulate truly long-term material degradation.

In this step, the tangential contact problem is neglected as it has a minor influence on the contact patch size, see, e.g. [16]. However, the tangential force from step 1 is applied in the calculation of damage in step 3.

(3) Simulation of damage evolution. Each load realization from the simulation of vehicle–track dynamics (step 1) and the corresponding contact simulation (step 2) constitutes one load cycle. One load sequence is defined by $N_1 \cdot N_{\text{axle}}$ load cycles, corresponding to $N_1 \cdot N_{\text{axle}}$ wheel passes with N_1 different wheel profiles. Since it is computationally infeasible to update the rail profiles after each wheel passage, the load sequence is repeated N_2 times to obtain a total load collective that is applied in each iteration of the methodology. This step includes a calculation of the following damage modes:

(a) Calculation of accumulated plastic deformation. A plane strain model is used for each of the sampled rail cross-sections. For each load cycle, the applied normal load is scaled using an iterative procedure such that the maximum von Mises stress is identical to the one obtained from the Hertzian-based metamodel in step 2. In this way, the 3D problem is approximated by a number of 2D problems to reduce the computational effort associated with a 3D analysis of plastic deformation in a crossing. The influence of this approximation on the results remains to be quantified in future work. The tractive force (computed in step 1) is applied assuming full slip. The calculation uses the Ohno-Wang cyclic plasticity material model [17] for the rail. The model is formulated for small strains. Three back stresses were included in the model (see [14] for more details) to reach a good agreement with the uniaxial cyclic stress-controlled ratcheting experiments [18].

(b) Simulation of wear using FASTSIM and Archard's model for sliding wear [19]. The input for this analysis is provided by the simulations of vehicle–track interaction in step 1.

In the present version of the methodology, the two damage mechanisms are assumed to be decoupled within each iteration of the methodology to simplify and speed up the simulation process, see also discussion in Section 3.

(4) For each sampled rail cross-section, superposition of profile change, which is used as input in the next iteration.

The methodology has been validated by comparing predicted rail profiles with those measured at Härad in Sweden [9] and Haste in Germany [20], and by comparing the distributions of predicted and measured damage at Zeltweg in Austria [6]. In particular, the Zeltweg study showed that the methodology is capable of accurate qualitative prediction of long-term plastic deformation and wear. Thus far, it has not been possible to perform a rigorous quantitative validation due to uncertainties in the input data that represent the actual conditions in the field (wheel profiles, axle loads and material data, to name a few) as well as the necessary assumptions (such as superposition of responses from each of the vehicle passages within each iteration) dictated by the high computational effort.

3. Case study

The turnout radius affects the crossing geometry since the designed crossing angle is inversely proportional to the selected turnout radius. Here, the described simulation methodology is applied to compare the predicted accumulated damage for three crossings with nominal crossing angles 1:12, 1:15, and 1:18.5 (from turnouts with curve radii 500, 760 and 1200 m, respectively). For a given combination of wheel profile and rail geometry, the different crossing angles generate different impact angles and magnitudes of impact loads during the transition from wing rail to crossing rail. For a chosen traffic situation, the results will provide a quantification of the reduction in crossing life due to the selection of a turnout with a smaller radius and thus a larger crossing angle.

The case study considered here is passenger traffic in the through route of the crossing panel in the facing move (traffic direction from switch panel to crossing panel). The vehicle–track interaction model was developed in the commercial multibody simulation software SIMPACK 2019x. It consists of a vehicle model and a parameterized turnout model that allows for the crossing angle to be altered. The crossing geometries are constructed from 15 sampled rail cross-sections that are the same for all crossing angles. The different crossing angles are obtained by uniformly altering the spacing distance between the cross-sections. The virgin rail cross-sections are the nominal measured profiles previously presented in [6]. The smaller crossing angle corresponds to a larger spacing between the cross-sections: 50 mm between cross-sections for the 1:12 crossing angle, 61.5 mm for the 1:15 angle and 77.5 mm for the 1:18.5 angle. The vehicle model is based on the Manchester benchmarks passenger vehicle model [21] with two bogies and a carbody. In a previous study [6], it was found that a model of a single bogie captures the relevant responses with sufficient accuracy. The single bogie model was therefore employed in this study. The vehicle speed and axle load are set to 90 km/h and 19.1 tonnes, respectively, while the wheel–rail friction coefficient is assumed to be 0.35. In this

study, these three parameters are taken as constant for all load cycles. The track is the 'TM2' model configuration described in [22].

Within each iteration of the methodology, step 1 involves the simulation of 250 cases of dynamic vehicle–track interaction in the railway crossing, where each case involves a unique measured wheel profile assigned to all wheels in the bogie model. The measured profiles have been sampled from Regina passenger trains in Sweden [23] and sorted by conicity such that a higher wheel number corresponds to a higher conicity. This yields a load sequence with 500 unique load cycles (each bogie has two wheelsets) that the crossing is subjected to. Subsequently, for each rail cross-section, the elasto-plastic normal contact problem (step 2) is solved for all load cycles using a metamodel with input data from each case of wheel–rail contact. In step 3, the simulations of plastic deformation and wear are performed independently. This implies that the interaction between the two damage mechanisms is neglected. For example, the predicted accumulated plastic deformation does not influence the material hardness used as input in the wear simulations. However, there is an implicit interaction in the sense that both mechanisms obtain their input via the simulations of dynamic vehicle–track interaction that considers the updated rail profiles due to the summed contributions from plastic deformation and wear. A further development of the methodology could be to let the material hardness in the wear model be a function of the current yield stress (in each iteration step), which varies over the cross-section. The simulation of plastic deformation relies on a material routine calibrated for hot-rolled manganese steel (see [14] for more details), while the wear model employs a wear ratio $k/H = 8.7 \cdot 10^{-14}$ m^2/N calibrated for the measured average wear rate of 140 mm^3/MGT in an explosion depth hardened manganese crossing. Note that the manganese steel in crossings is normally explosion depth hardened instead of hot-rolled. The principal difference between the two materials is that the explosion depth hardened steel has a higher yield limit near the surface, which gradually drops with increasing distance from the surface. Such characteristics are difficult to reproduce in the test specimens used in laboratory experiments. This is why, in this study, the yield limit in the material model has been modified to the average yield limit of explosion depth hardened manganese steel (580 MPa) reported by the crossing manufacturer. Table 1 presents the values of the material model parameters used in this study.

In [6], it was shown that several load sequences can be applied before updating the rail profiles for the next iteration of the methodology without losing a significant level of accuracy. Here, a load collective with five repeated load sequences, corresponding to up to 2500 load cycles (depending on how many of the wheel profiles make contact with a given rail cross-section), is applied in each iteration. This means that about 0.05 MGT of traffic is simulated per iteration. The same load collective is applied for the wear calculations.

Table 1. Material parameter values (Poisson's ratio ν is not calibrated; compressive yield limit σ_y^{compr} is modified) for the Ohno-Wang model of hot-rolled Mn13.

E	ν	σ_y^{tens}	C_1	γ_1	m_1	C_2	γ_2	m_2	C_3	γ_3	m_3	σ_y^{compr}
(GPa)	(-)	(MPa)	(MPa)	(-)	(-)	(MPa)	(-)	(-)	(MPa)	(-)	(-)	(MPa)
200	0.3	351	31760	708	2.40	15990	718	2.56	2310	0	2	580

4. Results

In this section, the accumulated rail damage after a traffic load corresponding to 65 MGT (1300 iterations of the methodology) is presented including results describing the evolution of wheel–crossing interaction, wear and plastic deformation. In this study, it was found that plastic deformation was the dominant reason for profile degradation over time, in particular for the first 40 MGT.

4.1. Wheel–crossing interaction

Figure 3 shows a top view of the transition zone of a crossing where the wheels make the transition from wing rail to crossing rail. The bottom figure presents the time-variant position of the contact on the rails for the leading axle of two different bogies with different wheel profiles. For the bogie with wheel profile 35, it is observed that the transition to the crossing rail takes place farther away from the theoretical crossing point (TCP) than when the bogie has wheel profile 235. This could be expected since, as was mentioned in the previous section, the wheels were ordered by conicity (profile 35 has a lower conicity than profile 235). The top figure plots the normal contact force along the crossing for the two cases. The wheel with the smaller conicity produces a higher impact force (denoted with a circle) than the wheel with the higher conicity, which transitions earlier.

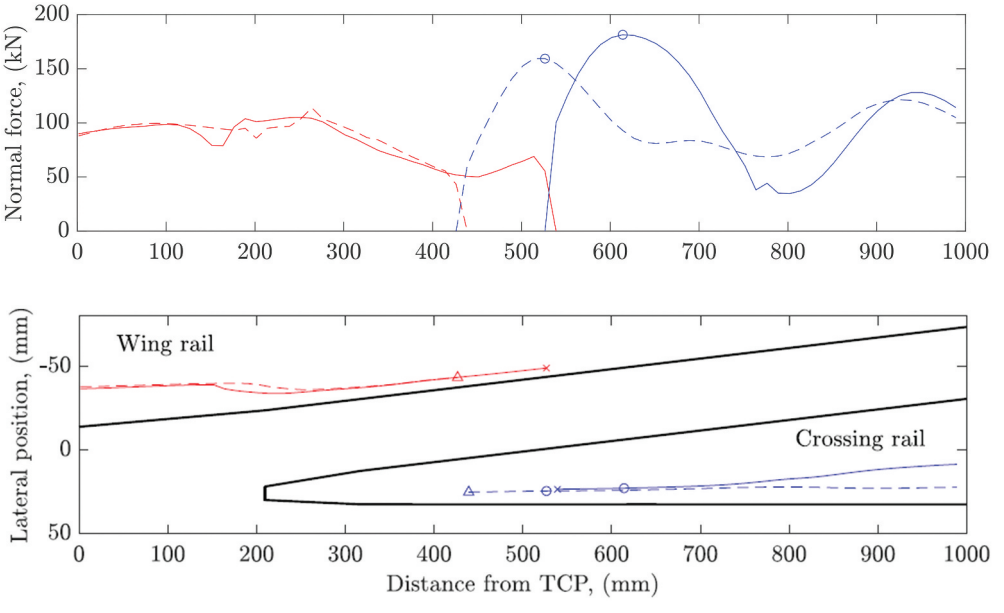

Figure 3. Illustration of wheel transition from wing rail to crossing rail with 1:15 crossing angle. Normal wheel–rail contact force (top) and contact position (bottom). Wheel 35 on wing rail is denoted by —— and on crossing rail by —— . Wheel 235 on wing rail is denoted by - - - and on crossing by - - - . Maximum normal forces and the corresponding contact positions on the crossing rail are circled. The corresponding points of contact on wing and crossing rails for wheels 35 and 235 at the transitions are denoted by a cross and a triangle, respectively.

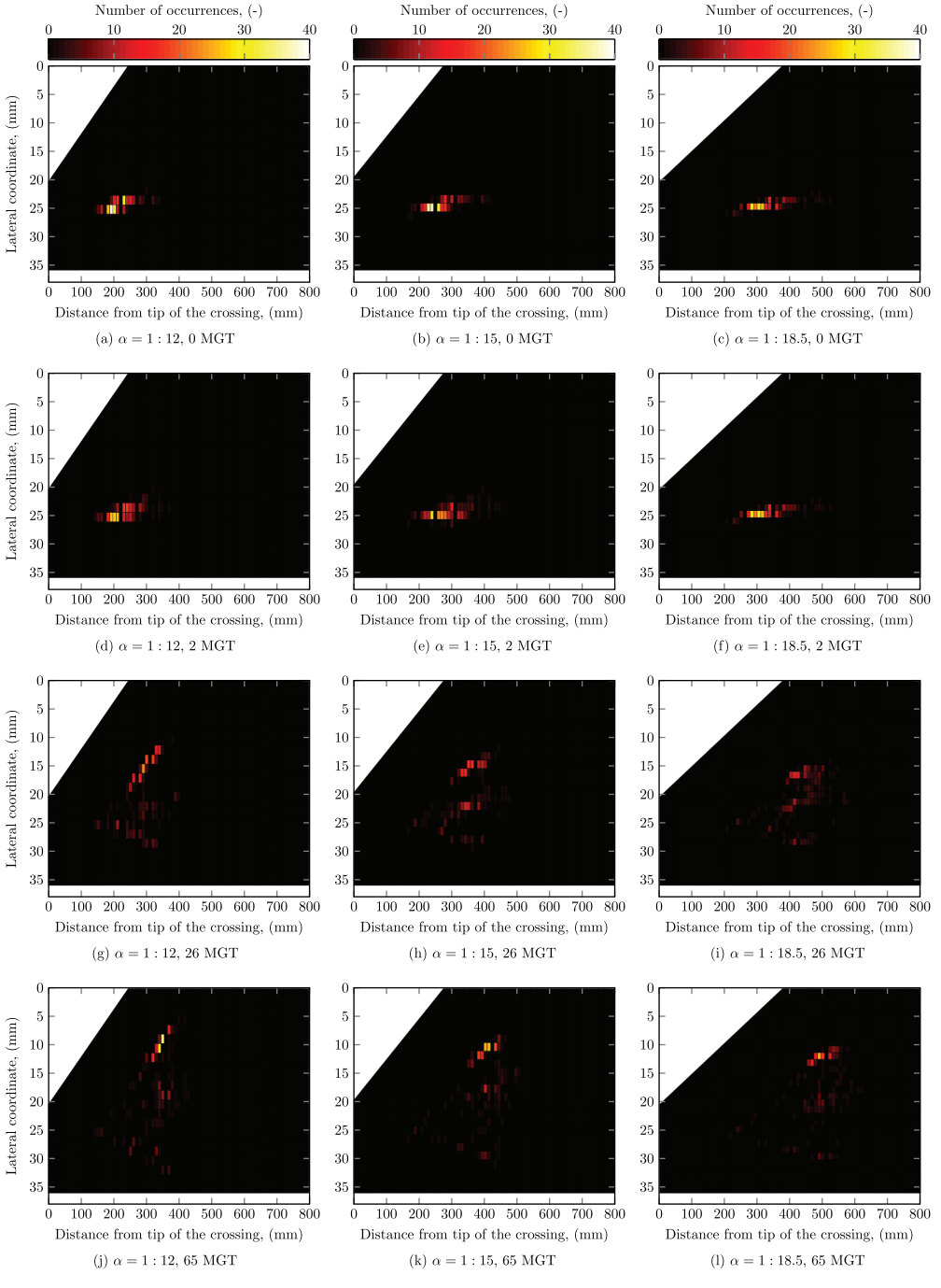

Figure 4. Influence of crossing angle and accumulated traffic load on the distribution of position of leading wheel transition (initial contact) to the crossing rail. In each subfigure, the accumulated number of leading wheels is 250.

Figure 4 presents a top view of the crossing rail. For each leading wheelset of 250 bogie passages, it illustrates the distribution of initial wheel–rail contact position after the

transition from the wing rail (exemplified by the coordinates of the left-most end of each blue curve in the bottom plot of Figure 3), and how it evolves over time for the three crossing angles. In each subfigure, the geometry has been discretised into a grid with cell side lengths 10.3 by 1.5 mm, and the number of occurrences of initial contact in each cell is shown. For the virgin geometry (0 MGT), Figure 4(a–c) illustrate that the wheel transitions take place at a lateral position of about 25 mm and that these are distributed over an extended length of the crossing rail with decreasing crossing angle. It is also observed that the wheel transitions occur at a longer distance from the tip of the crossing rail in case of a smaller crossing angle. Over time, due to degradation of the crossing rail, it can be noticed by comparing Figures 4(a)–Figures 4(l) that the transition zone becomes both wider and longer for all three geometries, although the length develops slower than the width. It becomes widest and shortest in the case of the largest crossing angle. The transition zone covering the longest distance is observed for the turnout with the smallest crossing angle, that is 1:18.5.

The corresponding evolution of the distribution of maximum normal contact force (the impact force value exemplified by the circle in the top plot of Figure 3) is presented in Figure 5. Initially, as for the position of the wheel transition shown in Figure 4, the distribution of the position (circled in the bottom plot of Figure 3) on the crossing rail corresponding to where the time history of the normal contact force has its maximum (magnitude of the impact load) is concentrated to a narrow region and is wider for the smaller crossing angle. The highest impact loads, however, are found further down the crossing, at the end of the marked region. Unlike in the previous figure, already after 2 MGT of traffic, the distribution becomes considerably wider and longer for all turnouts except the one with the 1:18.5 angle. At the same time, it is evident that the locations of the peak forces do not change much longitudinally. With more traffic passing through the crossings, the distribution of maximum normal force continues to grow wider, but it also starts to shift further down the crossing and splits into two clusters, set about 200 mm apart from each other. The magnitudes of the forces grow over time and peak at about 300 kN.

Based on the results of the simulations of vehicle–track interaction, the influence of the degradation of the crossing geometry can be indirectly examined by assessing the vertical wheel trajectory when transitioning to the crossing, see Figure 6. For a given wheel profile, it illustrates how the transition occurs later with increasing damage, but also how the magnitude of the wheel downward motion grows over time. This can be understood as an increase of the impact angle.

4.2. Wear

For each rail cross-section, the wear area A_w has been computed as the difference between the initial cross-sectional area A_0 and the current area A:

$$A_w = A_0 - A \tag{1}$$

For the three crossings, the distribution of A_w and its evolution over time are shown in Figure 7. As expected, for a given traffic scenario, it is evident that the crossing with a larger crossing angle α experiences more wear damage. Moreover, there is a more significant difference in the maximum of A_w between the crossings with the largest and

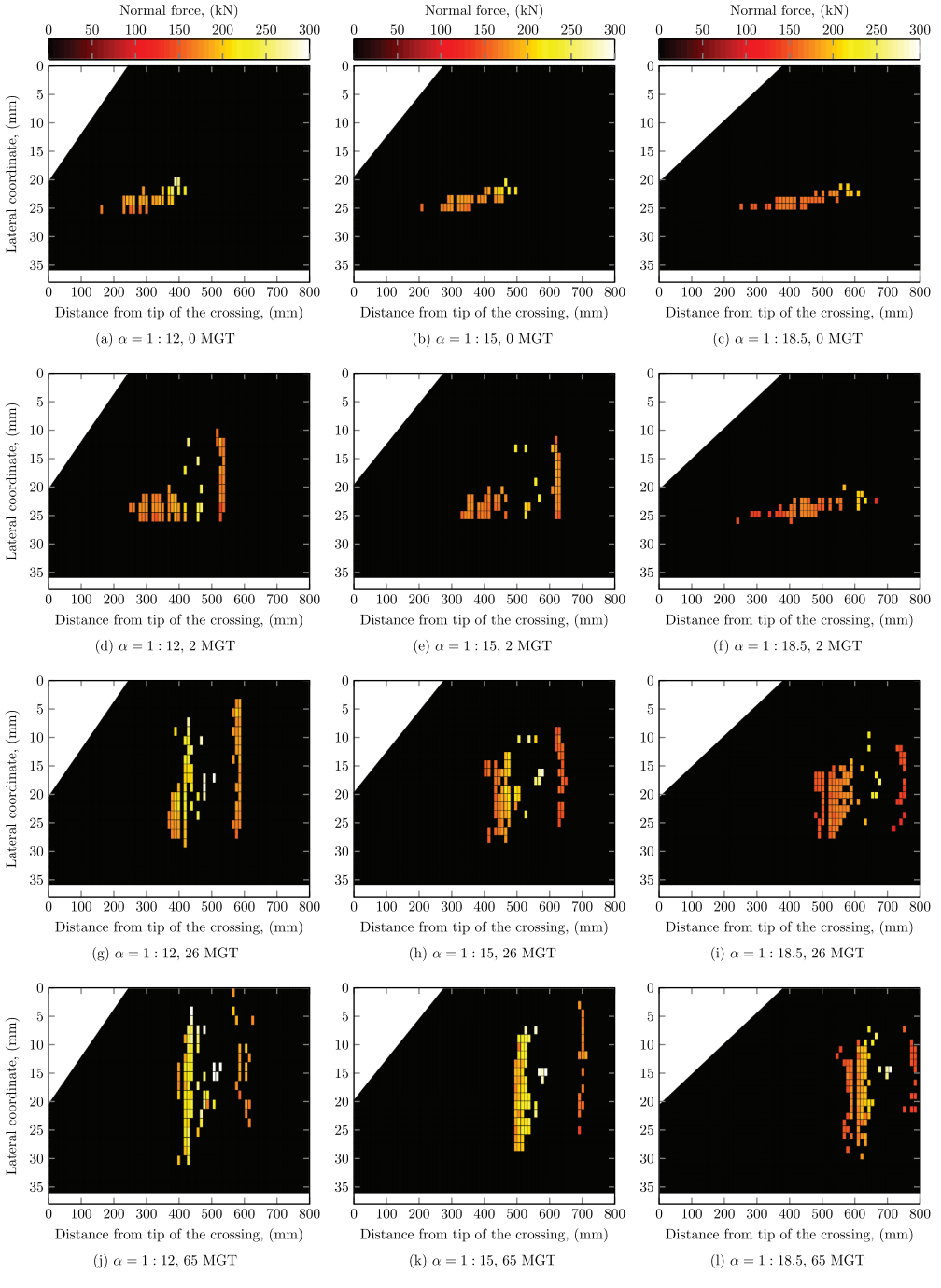

Figure 5. Influence of crossing angle and accumulated traffic load on the distribution of maximum wheel–rail normal force in the crossing for the leading wheel. In each subfigure, the accumulated number of leading wheels is 250.

medium α than between the crossings with the smallest and medium α, indicating a non-linear influence of crossing angle on wear. All three crossings exhibit three local maxima

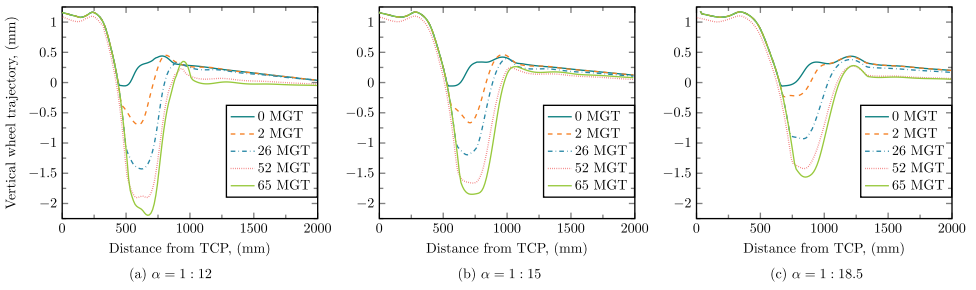

Figure 6. Evolution of vertical wheel (profile number 35) trajectory for three crossing angles.

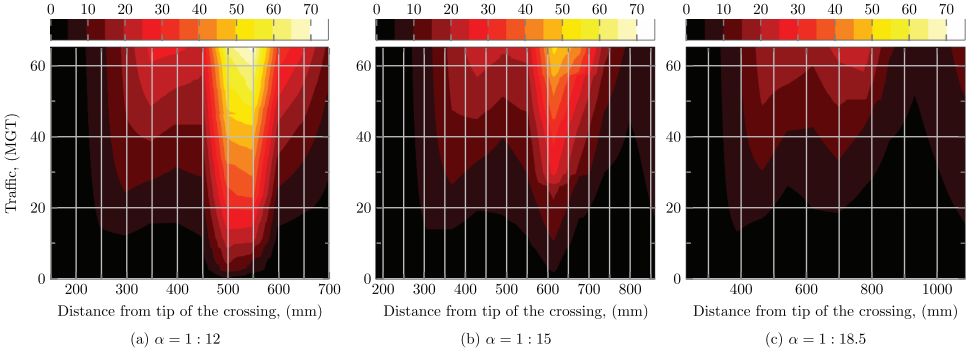

Figure 7. Distribution and time evolution of wear area, (mm^2). The data points are available for each of the 15 cross-sections with an increment of 0.5 MGT. Linear interpolation is applied in-between.

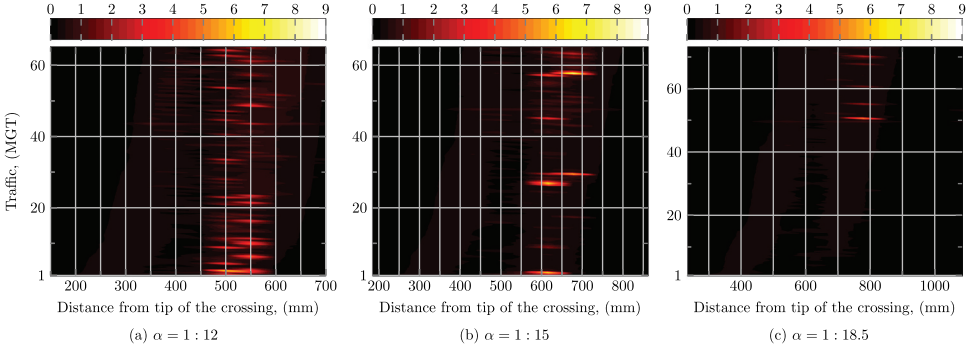

Figure 8. Distribution and time evolution of wear area rate, (mm^2/MGT). See also caption to Figure 7.

of A_w along their length. These maxima correlate well with the distribution of maximum normal forces shown in Figure 5. Figure 8 shows the evolution of A_w rates (wear area per MGT) over time for the three cases. The wear rate is nearly constant except for the first MGT (cf. the nested plot in Figure 11(b)). During the first MGT, the rates are approximately five times higher than later on. This is why these results were excluded from the figure to keep the resolution high enough to display the subsequent results. According to Archard's model of sliding wear [19], the wear volume V is proportional to the normal

load F_n and the sliding distance s, and inversely proportional to the hardness H of the softer material:

$$V = k\frac{F_n s}{H} \tag{2}$$

Throughout the simulations, the wear coefficient k and the hardness H were kept constant. This means that any predicted variation of wear rate would be due to changes in the normal force or sliding distance. Therefore, the nearly constant wear rate prediction observed in this study implies that the sum of all products $F_n \cdot s$ for a particular cross-section was nearly constant. This is in agreement with the wear and normal force plots in Figures 11(b) and Figures 12(c). It is worth noting that, for a given cross-section, the number of terms (number of wheels in contact) in the sum might vary over time.

4.3. Plastic deformation

In this study, the accumulated plastic deformation is found to be the dominant damage mechanism, both in the short term and long term. Partly, this is believed to be due to the material routine that has been calibrated for hot-rolled manganese steel, whose hardening is less pronounced compared to the explosion depth hardened manganese steel commonly used in crossings. In the adopted model, plastic strains are assumed to be incompressible and the volume of the material is therefore approximately not changed. Since the wear of each rail cross-section is determined by the area change, the shape change area is a selected complementary measure to quantify the plastic deformation. The shape change area A_u is defined as the sum of absolute rail surface displacements $\underline{u}_z$ excluding the wear area A_w:

$$A_u = \int |\underline{u}_z(y)| dy - A_w, \tag{3}$$

where y and z are Cartesian coordinates.

The evolution of the distribution of A_u over the crossing rail is shown in Figure 9. Similar to wear, the larger crossing angle corresponds to more damage. The plastic deformation is concentrated over a length of about 350 mm, regardless of the turnout

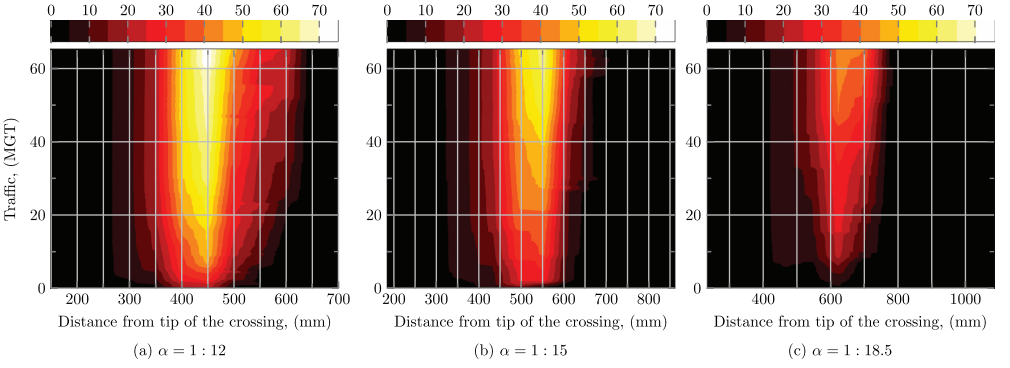

Figure 9. Distribution and time evolution of shape change area, (mm^2). See also caption to Figure 7.

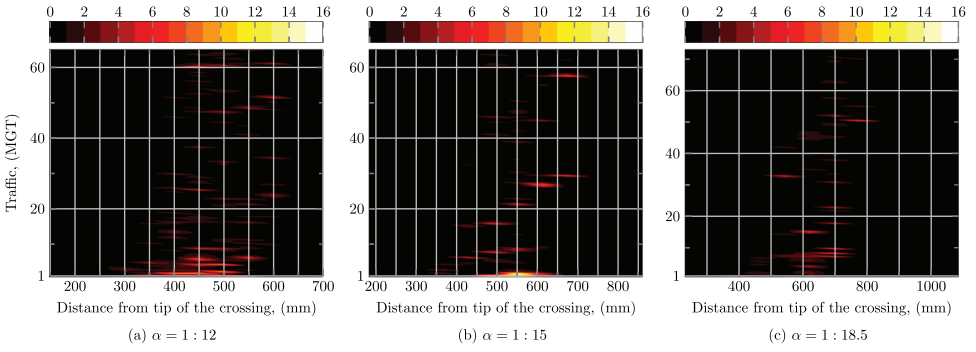

Figure 10. Distribution and time evolution of shape change area rate, (mm^2/MGT). See also caption to Figure 7.

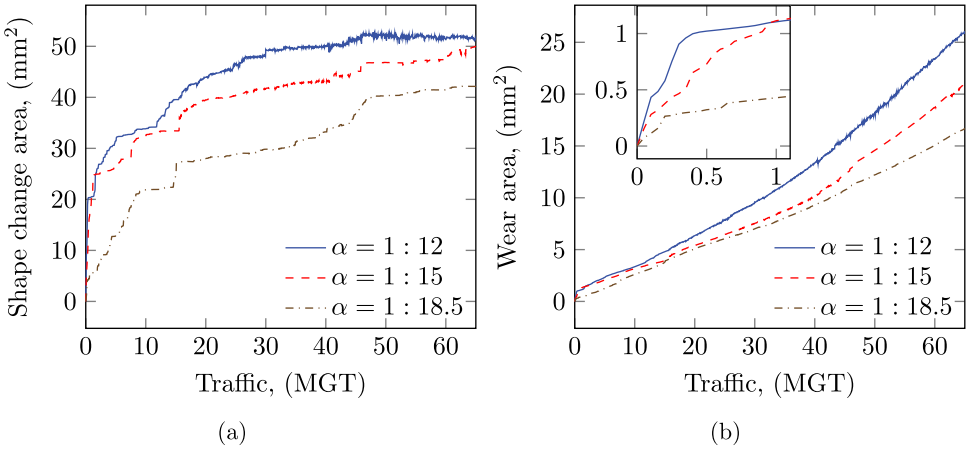

Figure 11. Shape change area (a) and wear area (b) for cross-section 9 at 400, 492 and 620 mm from the tip of the crossing for the 1:12, 1:15 and 1:18.5 crossing angles, respectively.

geometry (note the different ranges on the horizontal axes). The affected region grows over time as the wheel transitions occur later in the crossing and over a longer distance. When it comes to rates of plastic deformation, Figure 10 shows that the rates drop during the first 10–30 MGT, depending on the crossing angle, and then reduce to a nearly constant value below 5 mm^2/MGT.

For cross-section 9 (of the 15 sampled cross-sections that describe the geometry of the crossing) and the three different crossing angles, Figure 11 compares the evolution of accumulated plastic deformation and wear with increasing accumulated traffic load. Note that the location of each cross-section differs with the crossing angle. Cross-section 9 is located at 400, 492 and 620 mm from the tip of the crossing for the 1:12, 1:15, and 1:18.5 crossing angles, respectively. From the figure, it can be concluded that a larger α corresponds to higher rates of both shape change area (at least up to 30 MGT) and wear area. With increasing accumulated traffic load, the gradient of A_u is reduced and eventually becomes nearly zero for all three crossing angles, whereas the wear rate is relatively constant over time, except during the first MGT. Also, the figure gives another

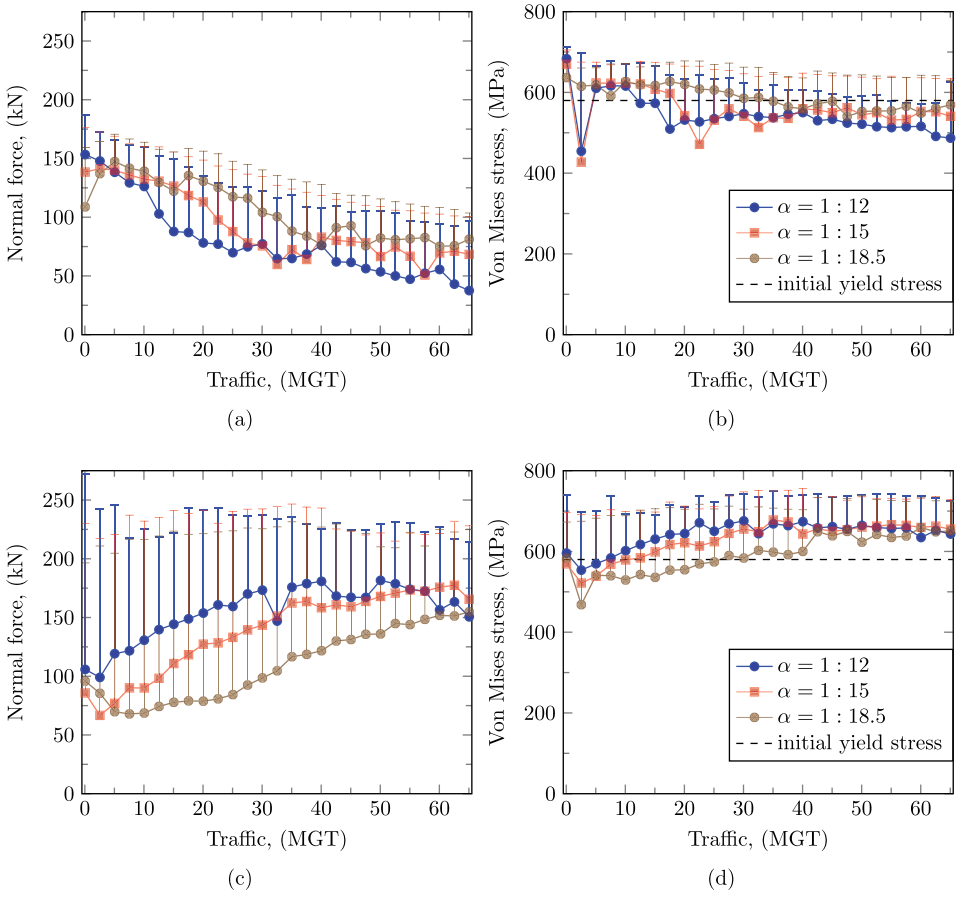

Figure 12. Normal force and maximum von Mises stress evaluated for all wheel profiles for cross-sections 7 (a, b) and 9 (c, d). Markers and bars denote median and maximum values, respectively. Cross-section 7 is at 300, 369 and 465 mm from the tip of the crossing for the 1:12, 1:15 and 1:18.5 crossing angles, respectively. See caption to Figure 11 for coordinates of cross-section 9.

perspective on the rate of A_u, as it can be seen that the gradient of each curve starts to approach a smaller value compared to the wear gradient after about 30–45 MGT, the value again depending on the crossing angle. The wear curves start to diverge over time, with a larger α leading to a faster increase of wear area.

For all the wheel passages on cross-sections 7 and 9, Figure 12 depicts the evolution of normal contact forces and maximum von Mises stresses. In Figure 12(a,c), it is observed that the median of the magnitudes of the normal force has opposite trends for the two cross-sections. This is in agreement with Figures 4 and Figures 5, which show that over time the wheel transitions from wing rail to crossing rail, as well as the positions of wheel–rail impact, are shifted further down the crossing. Thus, the degradation of rail profiles influences the dynamic interaction such that the most severe impacts move in the direction of travel. It can also be noted that the three crossing angles show opposite relations for the selected cross-sections. The 1:12 crossing leads to the highest forces in

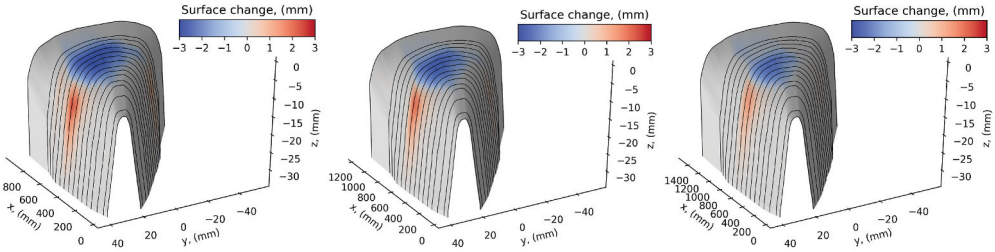

Figure 13. Normal surface change due to accumulated wear and plastic deformation after 65 MGT of traffic. Negative values represent inward direction.

the case of cross-section 7, while they are the lowest for cross-section 9. Furthermore, it is noted that for the more damaged cross-section 9 the magnitude of the normal force drops during the first 2–7 MGT before starting to increase.

A similar picture is observed for the maximum von Mises stresses, see Figure 12(b) and Figure 12(d). For both cross-sections and the first few MGT of traffic, the median values of the stress drop below the initial yield stress. This is followed by a fast re-establishment of the initial stress level, which either continues increasing, as in the case of cross-section 9, or reduces again after 15 MGT, as in the case of cross-section 7. Note that the maxima of the von Mises stress drives the evolution of plastic deformation. This is evident from the staircase character of plastic deformation in Figure 11. During the first 10 MGT of traffic, these maxima are almost the same for the two cross-sections, whereas the median values are lower for cross-section 9, which was subjected to more plastic deformation, recall Figure 9.

The combined contribution of plastic deformation and wear to the total surface change of the crossing is shown in Figure 13, where the surface change normal to the nominal profile surface is plotted after 65 MGT of simulated traffic. Negative values represent inward surface change. Unlike Figures 7 and Figures 9, it reflects on the spatial distribution of damage in the crossing, depicting the widening of the damage zone along the length of the crossing. As concluded above, the crossing with 1:12 angle is subjected to the highest magnitudes of damage, and a wider damage zone at the top of the rail compared to the crossings with smaller crossing angles.

5. Conclusions

A multidisciplinary simulation methodology that has been developed for the prediction of long-term accumulated rail damage in switches & crossings (S&C) has been applied for the simulation of plastic deformation and wear in three crossings associated with turnouts of crossing angles 1:12, 1:15, and 1:18.5. A material routine calibrated for hot-rolled manganese steel was used for the simulations of plastic deformation, while a wear coefficient calibrated for the average wear rate measured in an explosion depth hardened manganese crossing was employed for the simulations of wear. For the given combination of traffic scenario and crossing material, the plastic deformation was found to be the dominant damage mechanism. For the 15 sampled rail cross-sections, it was found that

the crossing with the largest crossing angle was subjected to about three times higher maximum wear and about two times higher maximum shape change area associated with plastic deformation than the crossing with the smallest crossing angle. The rates of plastic deformation decayed rapidly during the first 2–5 MGT of traffic and after about 10–30 MGT, depending on the crossing angle, started to approach values significantly lower than those of the wear rates. For each crossing angle, the wear rates were nearly constant throughout the entire simulation, showing a local redistribution of wear over time. Furthermore, for the given load sequence, the results suggest that the rail cross-section with the higher maximum value, but possibly lower median value, of the maximum von Mises stresses was subjected to more plastic deformation.

Acknowledgments

The current study is part of the ongoing activities in CHARMEC – Chalmers Railway Mechanics (www.chalmers.se/charmec). Parts of the study have been funded within the European Union's Horizon 2020 research and innovation programme in the project In2Track2 under grant agreement No 826255. The authors would like to thank voestalpine VAE GmbH and the Swedish Transport Administration (Trafikverket) for their support. The simulations were performed on resources at Chalmers Centre for Computational Science and Engineering (C3SE) provided by the Swedish National Infrastructure for Computing (SNIC). The choice of colour maps follows recommendations of Kenneth Moreland (see [24]).

Disclosure statement

No potential conflict of interest was reported by the authors.

Funding

This work was supported by the European Union's Horizon 2020 research and innovation programme in the project In2Track2 under grant agreement 826255.

ORCID

Rostyslav Skrypnyk http://orcid.org/0000-0001-7180-7280

References

[1] Dahlberg T, Ekh M, Nielsen JCO, et al. State-of-the-art study on railway turnouts: dynamics and damage. Gothenburg, Sweden: Department of Applied Mechanics, Chalmers University of Technology; Research report 2004; 2004. p. 8.
[2] Xin L, Markine V, Shevtsov I. Numerical procedure for fatigue life prediction for railway turnout crossings using explicit finite element approach. Wear. 2016;366-367:167–179.
[3] Pletz M, Daves W, Ossberger H. A wheel set/crossing model regarding impact, sliding and deformation – explicit finite element approach. Wear. 2012;294-295:446–456.
[4] Wiest M, Kassa E, Daves W, et al. Assessment of methods for calculating contact pressure in wheel-rail/switch contact. Wear. 2008;265(9):1439–1445.
[5] Su X, Clayton P. Ratchetting strain experiments with a pearlitic steel under rolling/sliding contact. Wear. 1997;205(1):137–143.

[6] Skrypnyk R, Ossberger U, Pålsson BA, et al. Long-term rail profile damage in a railway crossing: field measurements and numerical simulations. Wear. 2020. doi:10.1016/j.wear.2020.203331
[7] Gao Y, Wang P, Liu Y, et al. Investigation on wheel–rail contact and damage behavior in a flange bearing frog with explicit finite element method. Math Prob Eng. 2019:17. doi:10.1155/2019/1209352.
[8] Wang P, Xu J, Xie K, et al. Numerical simulation of rail profiles evolution in the switch panel of a railway turnout. Wear. 2016;366-367:105–115. Contact mechanics and wear of rail/Wheel systems, CM2015, August 2015.
[9] Johansson A, Pålsson BA, Ekh M, et al. Simulation of wheel–rail contact and damage in switches & crossings. Wear. 2011;271(1–2):472–481.
[10] Lagos RF, Alonso A, Vinolas J, et al. Rail vehicle passing through a turnout: analysis of different turnout designs and wheel profiles. Proc Inst Mech Eng F J Rail Rapid Transit. 2012;226(6):587–602.
[11] Bezin Y, Kostovasilis D, Sambo B. Reducing impact loads at railway crossings using tuned resilient elements. In: Klomp M, Bruzelius F, Nielsen J, et al., editors. Advances in Dynamics of Vehicles on Roads and Tracks: Proceedings of the 26th Symposium of the International Association of Vehicle System Dynamics, IAVSD 2019, August 12–16, 2019; Gothenburg, Sweden; 2020. p. 390–396.
[12] Pålsson BA. A linear wheel–crossing interaction model. Proc Inst Mech Eng F J Rail Rapid Transit. 2018;232(10):2431–2443.
[13] Skrypnyk R, Nielsen JCO, Ekh M, et al. Metamodelling of wheel–rail normal contact in railway crossings with elasto-plastic material behaviour. Eng Comput. 2019 Jan;35(1):139–155.
[14] Skrypnyk R, Ekh M, Nielsen JCO, et al. Prediction of plastic deformation and wear in railway crossings – comparing the performance of two rail steel grades. Wear. 2019;428-429:302–314.
[15] Kalker JJ. A fast algorithm for the simplified theory of rolling contact. Veh Syst Dyn. 1982 feb;11(1):1–13.
[16] Johnson KL. Contact mechanics. Cambridge, UK: Cambridge University Press; 1987.
[17] Ohno N, Wang JD. Kinematic hardening rules with critical state of dynamic recovery, part I: formulation and basic features for ratchetting behavior. Int J Plast. 1993;9(3):375–390.
[18] Schilke M Degradation of railway rails from a materials point of view [dissertation]. Gothenburg, Sweden: Department of Materials and Manufacturing Technology, Materials Technology, Chalmers University of Technology; 2013.
[19] Archard JF. Contact and rubbing of flat surfaces. J Appl Phys. 1953;24(8):981–988.
[20] Nicklisch D, Nielsen JCO, Ekh M, et al. Simulation of wheel-rail contact and subsequent material degradation in switches & crossings. In: Proceedings 21st International Symposium on Dynamics of Vehicles on Roads and Tracks; Stockholm, Sweden; August 17–21; 2009. p. 1–14 (available on CD).
[21] Iwnicki S. Manchester benchmarks for rail vehicle simulation. Veh Syst Dyn. 1998 sep;30(3–4):295–313.
[22] Pålsson BA, Nielsen JCO. Dynamic vehicle–track interaction in switches and crossings and the influence of rail pad stiffness – field measurements and validation of a simulation model. Veh Syst Dyn. 2015;53(6):734–755.
[23] Pålsson BA, Nielsen JCO. Track gauge optimisation of railway switches using a genetic algorithm. Veh Syst Dyn. 2012;50(sup1):365–387.
[24] Moreland K. Why we use bad color maps and what you can do about it. Electron Imaging. 2016;2016(16):1–6.